Particles Morphology and Surface Properties as Investigated by HRTEM, FTIR and Periodic DFT Calculations: from Pyrogenic TiO2 (P25) to Nanoanatase

Particles Morphology and Surface Properties as Investigated by HRTEM, FTIR and Periodic DFT Calculations: from Pyrogenic TiO_2 (P25) to Nanoanatase

L. Mino, G. Spoto, S. Bordiga, A. Zecchina

J. Phys. Chem. C (2012), 116, 32, 17008–17018

DOI: 10.1021/jp303942h

Particles Morphology and Surface Properties as Investigated by HRTEM, FTIR and Periodic DFT Calculations: from Pyrogenic TiO_2 (P25) to Nanoanatase

Lorenzo Mino*, Giuseppe Spoto, Silvia Bordiga, Adriano Zecchina

Department of Chemistry, NIS Centre of Excellence, and INSTM Reference Center, University of Turin, via P. Giuria 7, 10125 Torino, Italy

Abstract

By combining electron microscopy, FTIR spectroscopy of different CO isotopic mixtures and DFT calculations, a complete assignment of the IR spectrum of CO adsorbed on P25 (a mixture of 85% anatase and 15% rutile) at various dehydration states, on its pure rutile component and on nanoanatase was obtained. It is shown that the measurements at 60 K provide IR spectra of unprecedented quality and that the spectroscopic method is extremely powerful not only to study the surface Lewis and Brønsted acidity, but also to investigate the particles morphology. Indeed, as CO adsorbed on different faces is characterized by different stretching frequencies, the IR spectrum contains information on the exposed faces and hence on particles morphology. This information, combined with the study of the IR spectrum of CO adsorbed on defects, of dipole-dipole interactions between parallel oscillators adsorbed on extended faces and with HRTEM results, allowed us to fully explore the relations between particles morphology and surface properties. By comparing the spectra of CO obtained on P25, on the pure rutile fraction of P25 and on nanoanatase, the high crystalline character of P25 is inferred, which is likely the key of its outstanding photocatalytic activity. It is also found that the IR spectrum of CO on P25 is the sum of the rutile and anatase contributions and that no additional surface features ascribable to anatase-rutile junctions are noticeable, thus contributing to the strong debate present in literature.

Keywords: TiO_2, Degussa P25, anatase surfaces, FTIR of adsorbed CO, hydroxyl groups, electron microscopy, *ab initio* modeling.

Introduction

Since few decades the properties of TiO_2 phases anatase and rutile have been intensively investigated because of their wide applications in photocatalysis[1] and as photovoltaic cells components[2] and more than 7000 papers related to these topics have been published in the last 10 years.

As in most applications the surface properties are mainly involved, many efforts have been devoted to study single-crystalline TiO_2 surfaces using scanning tunnelling microscopy (STM),[3] atomic force microscopy (AFM),[4] low energy electron diffraction (LEED)[5] and surface X-ray diffraction (SXRD)[6] coupled with *ab initio* modelling.[7] The driving force for pursuing this kind of research is the expectation that insight into surface properties at the fundamental level will help to design materials with improved performances.

Nowadays the structure, the relaxations and the reconstructions of the most common rutile and anatase surfaces are well known,[8] but their correlation with the physicochemical properties, which are relevant for applications, is not always straightforward.

In the field of heterogeneous catalysis, for example, the problem of the outstanding activity of Degussa P25, which makes it a benchmark for testing new synthesized materials, is still under debate. Degussa P25 is a mixture of about 85% anatase and 15% rutile with a surface area of 60 m^2/g prepared by flame hydrolysis of $TiCl_4$. Its morphology has been deeply investigated by high resolution transmission electron microscopy (HRTEM),[9-12] highlighting that the main exposed surfaces are anatase (101) and (001).

Early studies suggested that the enhanced activity of P25 could be ascribed to the presence of a rutile layer on the surface of the anatase particles:[13] this hypothesis seemed highly attractive since rutile, being characterized by a band gap (3.0 eV) lower than anatase (3.2 eV), could more efficiently collect the sunlight and transfer the excitation to the underlying anatase phase.

However, as later HRTEM investigations have apparently demonstrated that P25 does not show the coexistence of more than one crystalline phase on each individual particle,[10] the previous hypothesis concerning the positive role of the rutile phase is weakened. Nevertheless, as a matter of fact, the presence of a very thin layer of a rutile phase partially covering the anatase surfaces could escape the HRTEM observation. For this reason further studies with physicochemical methods more sensitive to the local surface properties are necessary and our contribution aims at covering this gap.

While there is no agreement on the synergic role of the anatase and rutile phases, convergent opinion is emerging on the positive role of an efficient charge separation in determining the photocatalytic properties of P25 and two main explanations have been advanced.

Following the first one, the efficient charge separation could be the result of the highly crystalline nature of the two phases deriving from the elevated temperature reached by the particles during the flame hydrolysis process.[13] Due to such highly crystalline character, the defects concentration is minimized and the charge separation is consequently maximized since defects are known to favor charge recombination.[14] Time-resolved microwave conductivity (TRMC) measurements[14-16] tried to investigate the charge-carrier dynamics to support this hypothesis, but in the case of P25 the interpretation of the data is difficult since the response is the result of the contributions of two phases and rutile accelerates the decay of the global measured signal.[16]

The second proposed explanation (not in contrast with the previous one) is that the recombination is slowed down by an electron transfer from rutile to anatase.[17] However this process, being critically dependent upon the existence of an interface between the two TiO_2 phases, suffers the same uncertainties mentioned above when the HRTEM results have been discussed.

It is worth to comment at this point that charge separation in the bulk cannot be the sole factor influencing the photoactivity. It is a matter of fact that, once the charge separation has happened in the bulk because of the photon absorption, migration of the electron and hole to the surface of the

micro/nano crystals must occur where they are trapped on the surface ions or on adsorbed species (mainly OH groups).[18] So the question immediately arises about the role of different faces and surface hydroxyls in electrons and holes localization, a fact which in turn recall both the problem of the surface structures of the different faces and the problem of crystal morphology. These are other issues that will be addressed in this contribution.

From all these observations the importance of an accurate characterization of the different surfaces present in anatase, rutile and anatase-rutile mixtures is clearly emerging. In particular in this study the surface and bulk properties of native P25 (83% anatase and 17% rutile), of nanoanatase and of the rutile component of P25 are studied by means of several physical methods including BET surface area determination, XRD, HRTEM and FTIR of adsorbed CO. Concerning the last technique it is worth to recall that carbon monoxide is a very sensitive probe of the surface Lewis acidity since its stretching frequency is directly linked to the electrophilicity of the surface Lewis acid sites (Ti^{4+} centres) located on extended surfaces, edges, steps and corners. In fact the greater is the electrophilicity of the metal cation, the higher is the blue-shift with respect to the value in gas phase (2143 cm^{-1}).[19] In addition the CO molecule is also able to interact with surface hydroxyl groups via hydrogen bonding, so providing information about the acid character of hydroxyl groups present on extended faces and on defective situations like edges, steps and corners. Finally, since the stretching frequency of adsorbed CO is also strongly influenced by the lateral interactions occuring in the adlayers,[20] it can give indirect information on the bidimensional packing of Lewis centres and hence of the structure of the different adsorbing faces. In conclusion CO is not only an excellent probe of the individual sites, but can also give information about faces distribution and hence particles morphology.

Another advantage of the use of CO as probe of the surface sites and structures is related to the parallel and well established use of first principles calculations to evaluate the blueshift caused by the interaction with different surfaces.[21-26] In this contribution a systematic comparison of the experimental

and theoretical results is consequently performed. We will demonstrate that modelling is playing a fundamental and vital role in assisting the interpretation of the FTIR spectra of adsorbed CO and hence in understanding the properties of the different faces and structures present on anatase and rutile particles.

Experimental

Samples. Anatase nanopowder (hereafter nanoanatase) was purchased from Sigma-Aldrich and P25 from Evonik Industries (formerly Degussa). For some experiments, we tried to isolate the rutile component of P25 by etching the native material with hydrofluoric acid (HF). To this purpose, a 10% HF solution (400 mL) was prepared by diluting 40% hydrogen fluoride (Merck) with deionized water, then 10 g of P25 were added and the suspension was stirred for 12 hours. After the treatment, the etched TiO_2 particles (hereafter P25HF) were separated by centrifugation, washed with deionized water and heated in air at 500°C for 1 hour to remove the impurities before performing the characterization.

The phase composition, the particle dimension and the BET surface area of the investigated samples are reported in Table 1.

FTIR spectroscopy of adsorbed CO. Before CO adsorption the samples were outgassed under high vacuum (residual pressure < 10^{-4} mbar) in the same cryogenic cell (a closed circuit liquid helium Oxford CCC 1204 cryostat properly modified)[27] allowing the infrared investigation of species adsorbed in controlled temperature (between 300 and 14 K) and pressure conditions. After the thermal treatment, the samples were oxidized with 15 mbar of O_2 to obtain stoichiometric TiO_2. Then O_2 was outgassed at room temperature and 40 mbar of CO gas were dosed on the samples. The infrared spectra were recorded at 60 K on a Bruker Equinox 55 FTIR spectrometer, equipped with an MCT cryogenic detector, with the sample compartment modified to accommodate the cryogenic head; 128 interferograms (recorded at 2 cm^{-1} resolution) were typically averaged for each spectrum.

HRTEM. High-resolution transmission electron micrographs were obtained with a JEOL 3010-UHR instrument operating at 300 kV, equipped with a 2k × 2k pixels Gatan US1000 CCD camera. Samples were deposited on a copper grid covered with a lacey carbon film.

Field emission scanning electron microscopy. Field emission scanning electron (FESEM) micrographs were acquired with a Zeiss Supra 40 scanning electron microscope based on Zeiss GEMINI field emission SEM column. Samples were deposited on a copper grid covered with a lacey carbon film.

Adsorption of N_2 at 77 K. The surface area of the investigated samples was measured by adsorption of nitrogen at 77 K on samples pretreated at 423 K under vacuum, applying the Brunauer–Emmett–Teller (BET) equation. Measurements were performed with a Micromeritics ASAP 2020 sorption analyzer.

TGA. The thermogravimetric analysis was performed with a TA Instruments Q600 SDT. The sample was heated at 2 K/min under a 100 mL/min nitrogen flux.

XRD. X-Ray Powder Diffraction patterns have been collected in 3-80 2θ range, with angular resolution 2θ = 0.016 and integration time of 90 seconds per step, with a PW3050/60 X'Pert PRO MPD diffractometer from PANalytical working in reflection mode in Bragg-Brentano geometry. The source used was a high power ceramic tube PW3373/10 LFF with Cu anode, equipped with Ni filter to attenuate K_β. The scattered photons have been collected by a RTMS (Real Time Multiple Strip) X'celerator detector and the samples were hosted in amorphous SiO_2 holder.

The quantitative analysis of the anatase/rutile ratio in the samples was performed using the following equation:[28]

$$X_A = \left(1 + 1.26 \frac{I_R}{I_A}\right)^{-1}$$

where X_A is the weight fraction of anatase in the sample, I_R the intensity of the (110) rutile diffraction peak and I_A and intensity of the (101) anatase diffraction peak.

The (101) anatase reflection and the (110) rutile reflection were also exploited to calculate the average crystallite size with the Scherrer equation. The instrumental broadening was corrected using a Si powder standard.

Results and discussion

1) P25

1a) Morphology of the P25 particles

A HRTEM study of P25 particles morphology was performed in order to identify the most commonly exposed faces: low magnification images of P25 are shown in Figure 1a-b. These images do not represent a novelty as TEM images of the popular P25 photocatalyst are frequently reported in the literature.[10-12] Nevertheless they are shown again here to recall that the particles, although highly crystalline, are in form of irregularly shaped polyhedra and are so exposing several families of faces. The particles have size in the 10-50 nm range. This result is in agreement with the value of 26 nm obtained for anatase particles and 42 nm for rutile particles from the XRD data applying the Scherrer equation. To have an insight about the exposed faces of the most common anatase crystallites, a high magnification image of a nearly isolated particle is reported in Figure 1c. From this figure the high crystallinity of the particle is clearly emerging (as demonstrated by the presence of interference fringes) together with the coexistence of different facelets.

However, as the relative contribution of these faces is varying from one particle to the other, it is impossible to extract from the HRTEM results a shape of the mean polyhedron representing the P25 particles. Furthermore the apparent rounded profile of most particles suggest that, besides the (101), (001) and (100) faces, mentioned also in previous studies,[9,11,29] also the (112) and (110) surfaces could be present in a more limited extent. One conclusion is however emerging: the experimentally observed particle morphology is not fully compatible with the truncated bipyramidal shape (see Figure 1d) where

only the (101) and (001) faces are present, as predicted by *ab initio* calculations on anatase crystals in equilibrium conditions.[30] Other polyhedra (see Figure 1e) and hence a more complex faces distribution constituted at least by three predominant faces (i.e. 101. 001 and 100) and the less abundant (112) surface look definitely more appropriate to simulate the experimental contours of the particles (Figure 1a-b-c). This conclusion is confirmed by the examination of the interference fringes parallel to the particles edges present in several HRTEM images (e.g. in Figure 1c), where the (101) planes are by far the most abundant, followed in second position by the (100) and (001) and finally by the (112) ones. The complex shape of the P25 particles is certainly the result of a "non equilibrium morphology" due to the kinetic effects associated with the preparation method (flame hydrolysis) .

Little information can be obtained about the rutile crystals, which are less abundant and cannot be easily distinguished in the images. On the shape of the rutile particles present in P25 we shall return in the following when the morphology of the sample obtained by dissolving the anatase phase with a HF solution will be discussed. From Figure 1c it is also clear that the borders of the particles show often the presence of steps and corners which, although not representing the major fraction of the surface centres, are interrupting the extension of the faces planarity and can play a crucial role in the chemical reactivity.

Concerning the surface species present on the different faces and defects, coordinatively unsaturated Ti^{4+} centres (Ti^{4+}_{cus}), hydroxyl groups and molecularly adsorbed water must be considered. Ti^{4+}_{cus} with Lewis acid character are expected to be nearly absent on TiO_2 exposed to atmosphere, being covered by adsorbed water under molecular or dissociated form, and to show up only upon outgassing the sample under vacuum at proper temperatures.

The 5-fold Ti^{4+}_{cus} sites on flat surfaces and terraces should be the first to be formed upon loss of water, while 4-fold coordinated Ti^{4+} centres on edges and steps and finally 3-fold Ti^{4+} centres on corner positions should appear only at higher outgassing temperatures.

It is so evident that controlled dehydration at increasing temperature is a method which allows to gradually tune the surface properties and the progressive development of Lewis acidity.[29]

1b) Study of the dehydration of P25

The variation of the surface adsorbed water concentration as a function of the temperature was investigated by thermogravimetric analysis (TGA). The experimental details of the TGA results are described in the Supporting Information. To obtain a qualitative estimate of the percentage of surface Ti atoms free from adsorbed water (either in molecular or dissociated form) at increasing temperatures, the following formula was applied:

$$\%Ti_{hyd}(T) = \frac{W(T) - W_0}{\rho_{Ti} \cdot S_{BET} \cdot M_{H_2O} \cdot W_0} \cdot 100$$

where $\%Ti_{hyd}$ is the percentage of surface Ti atoms covered by adsorbed water, i.e. fraction of Ti^{4+}_{cus} = 1-(fraction of Ti_{hyd}), W(T) the weight of the sample measured at temperature T, W_0 the weight at the end of the ramp when the sample is expected to be completely dehydrated, ρ_{Ti} the density of surface Ti atoms, S_{BET} the BET surface area of the sample and M_{H_2O} the molecular mass of water

From the results reported in Figure 2a, it is possible to see that: a) in the RT-300°C interval, the fraction of Ti^{4+}_{cus} centres increases up to ~75% b) in the 300-500°C interval, the fraction of Ti^{4+}_{cus} undergoes a further increment reaching gradually ~85%. Notice that 500°C is the highest temperature at which the surface area and the rutile content remain unchanged during the TGA experiment.

On the basis of the literature results[29,31,32] and of the FTIR spectra illustrated below, we can safely assume that in the RT-300°C interval water molecularly adsorbed on extended faces is predominantly desorbed, while in the 300-500°C interval the progressive condensation of residual hydroxyl groups (with water elimination) located on the most reactive faces, on edges, steps, corners and other defects is progressively occurring. However not all water adsorbed on sites located on defects can be eliminated

upon heating at 500°C, but higher outgassing temperatures must be avoided since over 500°C the anatase-rutile transformation starts to occur.

The FTIR spectra reported in Figure 2b-c confirm the hypothesis that molecularly adsorbed water is the first to disappear. In fact, using the 1620 cm^{-1} band (bending mode of the water molecule) as indicator, it can be safely concluded that the molecularly adsorbed water is nearly completely removed upon outgassing the samples in the RT-300 °C interval. It is so evident that adsorption of CO probe (vide infra) on samples treated at 300°C will give information on the less reactive surfaces, i.e surfaces not able to adsorb water in dissociative form. At temperatures higher than 300°C the progressive hydroxyl groups condensation, leading to further water release, is starting to occur. This process, mainly involving the most reactive surfaces, edges, steps and corners should be accompanied by the gradual formation of new low-coordinated Ti^{4+} centres characterized by greater Lewis acidity and polarizing power.

Although it is outside the scope of this paper to discuss in details and assign the spectrum of adsorbed water on the sample treated at temperature lower than 400°C, we can remind that the broad absorption, extending from 3600 to 2500 cm^{-1}, and the signal centred at 1620 cm^{-1} (spectrum obtained at RT) are due to the ν(OH) modes perturbed by hydrogen bonding and to the δ mode of H_2O molecularly adsorbed on Ti^{4+} sites of faces and terraces. The narrow bands at 3632 and 3418 cm^{-1}, which have a similar behaviour, are likely due to unperturbed ν(OH) modes of water at the borders of the patches. A deeper discussion concerning these assignments can be found in literature.[29,31] Moreover theoretical studies assigned the bands in the 3620-3680 cm^{-1} region to water molecularly adsorbed on the (101) surface.[33].

At higher outgassing temperatures only two groups of bands in the 3750-3700 cm^{-1} and 3700-3600 cm^{-1} intervals can be observed, the latter being preferentially eroded upon increasing the dehydration time.

These absorptions are clearly originated by the superimposition of narrow components centered at 3722, 3678, 3662 and 3636 cm^{-1}.

The assignment of the two group of bands mentioned above is still matter of debate and their detailed assignment is outside the scope of this study. Experimentalists generally assert that the composite band above 3700 cm^{-1} is due to terminal hydroxyls, while the composite absorption at lower frequencies is ascribed to bridging hydroxyls.[32,34] Some calculations concerning hydroxyl groups on Ti atoms at edges have been performed adopting the harmonic approximation,[35] but unfortunately their comparison with the experimental data is not straightforward.

1c) The FTIR spectra of adsorbed CO: effect of surface hydroxylation

As the stretching frequency of adsorbed CO is very sensitive upon the perturbation caused by the interaction with the surface cations, it is evident that the IR spectroscopy of adsorbed CO represent an invaluable tool for the study of the Lewis acidity[36] and ultimately of the particle morphology since different faces should originate different CO bands.[19,26]

In our investigations CO was first adsorbed on a partially hydroxylated sample obtained by readsorption of approximately half monolayer of water on a sample previously outgassed at 500°C (Figure 3). The presence of molecular water on the surface is testified by the peak at 1620 cm^{-1} (inset of Figure 3a) and by the strong and complex absorption in the OH region (Figure 3b). As discussed before, in these conditions also the less reactive faces are partially covered by molecular water coordinated to fivefold coordinated Ti^{4+} sites, while the most reactive faces, the edges, steps and corners are nearly fully hydroxylated.

The relevant features of the spectrum of CO adsorbed at 60 K (Figure 3) are: a) a broad and highly reversible band at 2141 cm^{-1} due to physically adsorbed CO; b) a broad signal at 2148 cm^{-1}, shifting up to 2157 cm^{-1} at low coverage, originated by CO hydrogen bonded to OH groups[29] (either belonging to

molecular water or to hydroxyl groups formed on more reactive sites); c) a peak at 2179 cm^{-1} ascribed to CO adsorbed on fivefold coordinated Ti^{4+} sites not covered by adsorbed water.[11,19,29,37-39] The frequency of this peak is not changing with coverage (except a slight decrease in frequency at the highest coverages when the second CO layer starts to form) indicating that the CO oscillators are not interacting each other, probably because CO-CO (dipole-dipole) interaction is prevented because of the presence of coadsorbed water acting as a spacer.

A short treatment under vacuum at 400°C produces some interesting modifications on the spectrum of adsorbed CO (Figure 4): a) the bands due to hydroxyl groups show distinctly lower intensity and the bending mode of molecular water at 1620 cm^{-1} is absent (see inset of Figure 4a); b) in parallel the broad absorption in the 2152-2158 cm^{-1} range, assigned to CO interacting with residual OH, decreases; c) the same occurs for the complex absorption in the 3750-3600 cm^{-1} range due to the ν(OH··CO) species; d) the CO interaction induces a larger downshift of the stretching frequency for bridging OH groups (3700-3600 cm^{-1} interval in Figure 4b) than for terminal species (3750-3700 cm^{-1} interval in Figure 4b) suggesting an higher Brønsted acidity for the former species; e) the absorption of CO adsorbed on Ti^{4+}_{cus} is becoming more intense and complex. In particular, two bands are observed at 2179 (strong) and 2165 (very weak) cm^{-1}, which can be reasonably assigned to CO adsorbed on fully dehydrated patches on two different faces. In favour of this hypothesis is their progressive upward shift while decreasing coverage, which is indicative of the building up of lateral interactions between parallel CO oscillator adsorbed on bidimensional arrays of Ti^{4+} centres.

When the dehydroxylation process is pushed to the limit permitted by the anatase-rutile transformation by prolonged outgassing at 500° C, we reduce the hydroxyls coverage to about 15%, as highlighted by the TGA analysis. The corresponding CO spectra are reported in Figure 5 and the following can be commented: a) all the manifestations associated with hydroxyl groups before (bands in the 3750-3650 cm^{-1} interval) and after interaction with CO (broad bands in the 3650-3450 cm^{-1} interval) are

weakened; b) the higher acidity of bridged OH groups is confirmed; c) the spectrum of adsorbed CO is intensified and is now constituted by several bands.

Considering the maximum coverage (black curve in Figure 5a), we can notice that: i) the intensity of the band at 2179 cm^{-1} is essentially unchanged, thus suggesting that the associated face was already free from adsorbed water after short outgassing at 400°C; ii) the band at 2165 cm^{-1} triplicates its intensity iii) a pronounced shoulder grows up at ~ 2185 cm^{-1}; iv) a weak and narrow peak at 2175 cm^{-1} becomes evident; v) two narrow components at 2149 (w) and 2137 (sh) cm^{-1} appear, being no more obscured by the broad band due to CO interacting with OH groups; vi) very weak bands at 2212 (vw), 2208 (vw) and 2195 (sh) cm^{-1} show up.

The band at 2208 cm^{-1}, which is hardly reversible upon outgassing (see inset of Figure 5a), is characteristic of sites with larger polarizing power ($\Delta\nu$ ~ 70 cm^{-1}) as expected for 3-fold and 4-fold Ti^{4+} centres located on defects. Its intensity is very low, in agreement with the expected low concentration of these sites, and it is the last to disappear while outgassing, thus indicating that we are dealing with very stable species. Moreover, as expected, its intensity grows when increasing the dehydration time.

The band at 2212 cm^{-1} is more easily reversible: hence its attribution to defective sites is debatable. An alternative plausible assignment is in term of a combination mode involving the ν(CO) mode responsible for the main peak at 2179 cm^{-1} and a very low frequency mode of CO molecules adsorbed on facets.[40] Combination modes between a ν(CO) and a ν(Metal··CO) have been found for CO interacting with cations in zeolites[41] and for CO adsorbed on MgO.[27] However, from our periodic DFT calculations (see the Supporting Information for the computational details) we obtain values around 100 cm^{-1} for the ν(Ti··CO), therefore the titanium-carbon stretching vibration cannot be involved in the band at 2212 cm^{-1}, which should be originated by the combination of ν(CO) with another low frequency external mode with bending character.

The weak band at 2137 cm^{-1}, being characterized by a frequency lower than that of CO gas cannot be interpreted in terms of CO adsorbed via carbon end on Ti^{4+} centres. We shall return on its assignment in the following when the spectrum of CO adsorbed on the rutile component of P25 will be discussed.

All bands of the 2179-2149 cm^{-1} group undergo an upward shift upon decreasing the coverage. This shift is maximum for the 2179 cm^{-1} band and the 2185 cm^{-1} shoulder (+12 cm^{-1}), it is +6 cm^{-1} for the 2165 cm^{-1} peak and only +3 cm^{-1} for the 2149 cm^{-1} band. The observed shifts for the 2179 and 2185 cm^{-1} components are in rough agreement with the calculated values obtained by periodic DFT calculations.[26] Also the other bands (with exception of the 2137 cm^{-1} one) are shifting: however the shift value cannot be determined with precision because of the strong overlap with adjacent stronger bands. From these data, we can conclude that the effect of dipole-dipole interaction progressively decreases for surfaces showing a lower blueshift in the CO stretching frequency.

In conclusion, assuming that the five bands in the 2185-2149 cm^{-1} range are due to different facelets and that the extinction coefficient of adsorbed CO is almost constant in this interval, the morphological message given by the CO probe suggest that the facelets responsible for the 2185-2179 cm^{-1} bands are by far the most abundant (~80%), followed by those associated with the 2165 (~15%) and 2149 cm^{-1} peaks and ultimately by the 2175 cm^{-1} one. In the following we will prove that the 2149 cm^{-1} band is due to CO on rutile phase, therefore we can conclude that the anatase particles mainly expose four different families of facelets.

From the above discussion, we can infer that the 2179 cm^{-1} peak is due to the (101) face, which is the most frequently observed in the HRTEM images. Concerning the other surfaces, no straightforward assignment is possible at the moment, therefore only the comparison with computational results can clarify this point.

1d) The adsorbate-adsorbate interaction of CO oscillators on the different faces of P25

As already briefly discussed in the previous section, the spectroscopic response of the CO oscillators present on extended faces of oxides depends both on the Lewis acidity of the adsorbing centre and on the surface coverage (θ). In fact, while at low coverages CO oscillators on extended faces or terraces are isolated (singletons) and give only information about the acid strength of the sites, for CO coverages approaching the monolayer (θ = 1), they form patches of increasing size of parallel oscillators whose frequency is becoming influenced by static and dynamic interactions.

The dipole–dipole coupling between the adsorbed CO molecules gives rise to the dynamic interaction, while the static one depends upon the ability of the adsorbed molecules to transmit negative charge to the neighbouring adsorption sites.[42]

It is well known that on oxides the shift induced by dynamic effects ($\Delta\nu_{dyn}$) is positive, while that induced by static perturbations ($\Delta\nu_{st}$) is negative.[20,42] Static and dynamic effects depend upon the packing density of the oscillators and by their relative orientation. In particular the dynamic coupling is greatly reduced when adjacent oscillators are not parallel.[42]

In conclusion, the observed shifts with CO coverage of the 2179 and 2165 cm^{-1} bands are originated by the sum of two opposite effects (static and dynamic). In order to separate the two effects, the use of isotopic mixtures ($^{12}C^{16}O$-$^{13}C^{16}O$-$^{13}C^{18}O$ in our case) is needed. In fact a diluted isotopic CO oscillator characterized by a reduced mass higher than that of the most abundant $^{12}C^{16}O$ is fully dynamically decoupled and consequently its shift upon coverage changes is determined by the static effect only.

In order to investigate these problems, the FTIR spectra of a mixture containing ~ 65% $^{12}C^{16}O$, ~ 30% $^{13}C^{16}O$ and ~ 5% $^{13}C^{18}O$ adsorbed on a sample shortly outgassed at 500°C have been studied (Figure 6).

As visible in Figure 6a-c, the signal of the $^{13}C^{18}O$ fraction interacting with Ti sites located on the (101) surface shifts from 2075 to 2090 cm^{-1}. As these species are highly diluted in the more abundant $^{12}C^{16}O$ and $^{13}C^{16}O$ isotopes and hence fully dynamically decoupled, we can conclude that $\Delta\nu_{st}$ = -15 cm^{-1}. Considering the corresponding signal for the fully coupled $^{12}C^{16}O$ oscillators, which shifts from 2179 to 2191 cm^{-1}, we can infer that $\Delta\nu_{dyn}$ = +3 cm^{-1}. The band ascribed to $^{13}C^{16}O$ molecules (Figure 6a-b) confirms the above reported analysis showing a global shift of -14 cm^{-1}, suggesting that the $^{13}C^{16}O$ oscillators are only partially dynamically decoupled.

With a similar procedure we can obtain the shifts associated with the dynamic and static effects for the 2165 cm^{-1} peak: $\Delta\nu_{dyn}$ = +2 cm^{-1}, $\Delta\nu_{st}$ = -8 cm^{-1}.

The calculated shifts are comparable to those observed for CO adsorbed on MgO ($\Delta\nu_{dyn}$ = +3.5 cm^{-1}, $\Delta\nu_{st}$ = -11.3 cm^{-1}),[36] ZnO ($\Delta\nu_{dyn}$ = +6 cm^{-1}, $\Delta\nu_{st}$ = -28 cm^{-1})[20] and NaCl ($\Delta\nu_{dyn}$ = +3 cm^{-1}, $\Delta\nu_{st}$ = -6 cm^{-1}),[43] i.e. on solid surfaces where the electrostatic interaction is dominating.

2) Nanoanatase

Because of the absence of the rutile phase, of the very high surface area and of the associated presence of an abundant fraction of defect sites, nanoanatase seems to be the ideal system to validate the conclusions drawn from P25.

From the HRTEM images shown in Figure 7c, we can notice that the particles have size in the 5-20 nm range. This result is in agreement with the BET surface area (140 m^2/g) and the XRD average particle dimension (16 nm). Owing to the very irregular shape of the nanocrystals, nothing can be inferred about the prevalently exposed facelets, whose extension is however expected to be much lower than the corresponding faces of P25. On the contrary, it is evident that the defects (edges, steps and corners) population is considerably larger with respect to P25, as testified by the very irregular contours of the particles.

The FTIR spectra of adsorbed CO presented in Figure 7a-b reflect the highly defective morphology and the absence of the rutile phase. Indeed, the intensity of the bands in the 3750-3600 cm^{-1} range, due to OH groups on defects (edges, steps and corners), is larger than that found on P25 treated in a similar conditions. At the same time, the signals originated by CO on coordinatively unsaturated Ti^{4+} centres are weaker and broader with respect to P25. These observations are in accordance with the morphological observations which indicate a larger amount of defective sites with respect to P25 and a corresponding smaller extent of flat terraces and surfaces.

It is worth to note that the peaks at 2149 and 2137 cm^{-1} observed on P25 are fully absent: this suggests that they are associated with the rutile phase (vide infra) .

The shape and number of bands in the 2210-2169 cm^{-1} range are similar to those found on P25. The major difference is the lower intensity of the peak at 2179 cm^{-1} which implies that the corresponding face is less dominant.

Concerning the OH groups, we can notice that in nanoanatase the peaks in the 3750-3700 cm^{-1} interval are more intense with respect to those in the 3700-3600 cm^{-1} range (see Figure 7b), while we observe an opposite behavior in P25 treated in the same conditions. Since in nanoanatase the fraction of sites in corner position is higher, this observation seems to confirm the attribution of these species to terminal OH groups. The study of the perturbation of the stretching mode of hydroxyls upon interaction with CO highlights also an higher Bronsted acid character of the bridged OH groups with respect to the terminal ones.

3) Comparison with periodic DFT calculations

From the above reported discussion it is clearly emerging that, owing to the presence of several superposed components, it is not possible to unequivocally assign the different IR bands of adsorbed

CO on the basis of the HRTEM images and the FTIR spectra only. Therefore a close comparison of the experimental spectra with first principles calculations is needed.

In our recent paper[26] the optimized structure of the most commonly exposed anatase surfaces was obtained from periodic DFT calculations. These structures are illustrated in Figure 8.

The Ti^{4+} sites located on the different faces, although all 5-fold coordinated and hence exposing a single coordination vacancy, are not equivalent from the point of view of the polarizing power since they are shielded in a different way by the surrounding oxygen ions and since the covalent character of the surface bonds is varying from one face to the other. Indeed, the computed electrostatic potential at the position corresponding to the center of mass of CO in the adsorbate/slab system progressively increases from 0.16 V for the (001), to 0.33 V for the (100), to 0.43 V for the (101) and to 0.48 V for the (112) surface.[26] Therefore it is expected that the stretching frequency of CO probe adsorbed on them can vary from one face to the other. This issue has been addressed in the same contribution[26] and it was showed that the calculated ν(CO) frequencies for the (101), (100) and (112) surfaces are all grouped in a narrow interval (2185-2175 cm^{-1}) and that only the ν(CO) of CO adsorbed on the (001) face has a distinctly lower frequency. As the experimental spectrum of adsorbed CO is precisely constituted by an intense envelope of three bands in the 2185-2175 cm^{-1} interval and by one well separated component at 2165 cm^{-1}, we think that a strict analogy between the experimental and computational results is existing which can be exploited for the final assignment of the IR spectrum of adsorbed CO.

In order to fully assign the spectrum of CO obtained on highly dehydroxylated samples, it must also be added that the Ti^{4+} ions on edges, steps and corner positions are in a lower coordinative state (4-fold or 3-fold) than the ions located on planar surfaces (5-fold). These less abundant sites are so expected to show higher Lewis acidity and polarizing power with respect to sites located on planar surfaces.

Consequently CO adsorbed on these sites should originate weak bands at frequency higher than those characteristic of extended faces.

On the basis of the comparison of the whole series of experimental and computational studies the following complete assignment is emerging which is illustrated in Figure 9:

1) The weak shoulder at 2137 cm^{-1}, which is redshifted with respect to CO in gas phase, can be originated by CO molecules interacting through the oxygen atom[44] with Ti sites located on rutile particles (see Section 4 for further details).
2) The intense, broad and easily reversible band at 2140 cm^{-1} is readily ascribed to physically adsorbed CO forming a surface multilayer.[45]
3) The sharp peak at 2149 cm^{-1} gradually shifting up to 2152 cm^{-1} with coverage is originated by the interaction of CO with a facelet of the rutile component present in P25. This assignment is supported by fact that this peak is absent on nanoanatase and it is the dominant feature in the FTIR spectra of the rutile sample obtained by etching P25 with an hydrofluoric acid solution (vide infra).
4) The broad band in the 2154-2157 cm^{-1} range is due to CO interacting with residual OH groups located on edges, steps and corners. Indeed, its intensity decreases in samples containing less hydroxyl groups and its presence is associated with a parallel perturbation of the OH bands, as discussed in Section 1c.
5) On the basis of the comparison with computation results, the weak peak at 2165 cm^{-1} can now be safely assigned to CO adsorbed on (001) facelets. This band is only showing up when outgassing at high temperatures in agreement with theoretical studies[33,46] which showed that the (001) surface strongly adsorbs water in a dissociative way .
6) The main component at 2179 cm^{-1} of the group of overlapped signals in the 2185-2175 cm^{-1} range can be ascribed to CO interacting with Ti sites located on flat (101) surfaces. This assignment, although slightly different with respect to that proposed in our previous article,[26] is anyway

compatible with the DFT results and it is supported by very recent single crystal results[47] and by the HRTEM results which suggest that the (101) is the most abundant exposed surface.

7) The shoulder initially observed at about 2185 cm^{-1} can be assigned to CO adsorbed on Ti Lewis sites located on less extended faces like the (112) and (110).
8) The shoulder centered at 2175 cm^{-1} can be tentatively ascribed to CO adsorbed on flat (100) surface, which seem to be present in a more limited extent in the HRTEM images and shows a slightly lower calculated ν(CO).[26]
9) The weak signal at 2208 cm^{-1} is due to CO adsorbed on highly acidic Ti Lewis sites exhibiting very low coordination like those located on edges, steps and corners. The assignment to corner sites is further confirmed by our DFT calculation on the (103) surface which, although exhibiting 4-fold coordinated sites (like those located on edges), shows a $\Delta\nu$(CO) = 48 cm^{-1} at full CO coverage (see the Supporting Information for the computational details). This value is only slightly higher compared to the computed shifts reported in our previous article[26] for the (112) and (101) surfaces, i.e. $\Delta\nu$(CO) = 43-44 cm^{-1}. These results seem to support the assignment of the shoulder located at about 2195 cm^{-1} to CO adsorbed on edge sites.

It is worth to underline that the low temperature adopted for the FTIR experiments (60 K) allowed us to obtain spectra of improved quality (experimental data already present in literature are all recorded at a real temperature of 100 K or higher),[11,19,37,40,44,48-50] thus clearly identifying and assigning for the first time the FTIR signal at 2149 cm^{-1} to CO adsorbed on the rutile fraction of P25.

4) The rutile particles of P25

In the previous paragraphs we have anticipated that the 2149 and the weak 2137 cm^{-1} bands are due to CO adsorbed on rutile. So far the only experimental proof of this statement was based on the observation that these peaks are totally absent on nanoanatase.

In order to strengthen the assignment we studied the spectrum of CO adsorbed on the rutile fraction present in P25. The pure rutile phase was obtained by performing an etching with an hydrofluoric acid solution, which is able to totally dissolve the anatase particles, leaving the pure and possibly unaltered rutile component.[12]

The FESEM and HRTEM images reported in Figure 10b-c of the rutile nanocrystals obtained by this procedure show highly crystalline particles exposing well defined faces. A separate contribution, devoted to the relation between the morphology of rutile and the spectroscopy of adsorbed CO, will present a more precise determination of the morphology of these particles. Notice that some of the particles in the high resolution image in Figure 10c show a rounded profile. This could be the sign that also the rutile particles have suffered some edging effect during the treatment with the HF solution.

The sequence of FTIR spectra of adsorbed CO are very informative on the surface properties of the rutile fraction present in P25 (Figure 10a). In particular, besides the band due to CO interacting with OH groups (broad absorption at 2160-2158 cm^{-1}) and to physically adsorbed CO (2140 cm^{-1}) the spectra of CO on rutile are dominated by the following features:

1) A complex and broad absorption in the 2205-2175 cm^{-1} range, whose maximum is gradually moving upward (+12 cm^{-1}) while decreasing coverage. This band, plausibly due to the superposition of several components, is very similar to that observed on anatase. Assuming that all anatase components has been eliminated by the HF treatment, the complex 2205-2175 cm^{-1} absorption can be assigned to CO adsorbed on predominant faces of rutile. On this point we shall return in a future contribution specifically devoted to the CO-rutile system. This absorption is likely present also in the spectrum of CO on native P25, but,

owing to the considerably smaller overall surface area of the rutile component, it is overshadowed by the more intense spectrum of the anatase fraction, thus preventing its quantitative determination.

2) A weak shoulder at 2205 cm^{-1} due to a component very resistant to outgassing, as expected for CO adsorbed on low coordinated sites present on defects.

3) Two narrow peaks at 2149 and 2137 cm^{-1}. The first peak moves upwards (+3 cm^{-1}) when decreasing coverage, while the second peak is not affected by coverage. These peaks, which are totally absent on pure anatase and present with reduced intensity on the P25 spectra, can be considered as the fingerprint of rutile. The frequency of the 2149 cm^{-1} peak is only slightly blueshifted with respect to CO gas: this indicate that this particular rutile surface exposes Ti^{4+} centres characterized by very low polarizing power. Concerning the 2137 cm^{-1} peak, which falls at a frequency lower than that of the CO gas, the assignment to CO molecules interacting through the oxygen atom seems plausible.[44]

Conclusions

The combination of electron microscopy and FTIR spectroscopy of adsorbed $^{12}C^{16}O$, $^{12}C^{16}O$-$^{13}C^{16}O$ and $^{12}C^{16}O$-$^{13}C^{16}O$-$^{13}C^{18}O$ isotopic mixtures allowed us to achieve a comprehensive characterization of the surface properties of P25 and nanoanatase. The complete assignment of the FTIR spectra of adsorbed CO on P25 was performed on the basis of morphological observations and periodic DFT calculations.

It is demonstrated that the FTIR spectra of adsorbed CO represent a very powerful tool not only to study the Lewis and Brønsted sites present on the different faces and defects, but also to investigate the particles morphology. In fact, as the stretching frequency of adsorbed CO depends upon the face indexes, the FTIR spectrum is providing information on the number and the extent of the exposed surfaces and on the defective sites and hence ultimately on the particles morphology. This approach, in

combination with HRTEM and DFT calculations, can overcome many of the limitations encountered by the classical single crystal surface science techniques (e.g. STM, AFM) when they have to deal with high surface area polycrystalline materials, which are widely employed in technological applications.

We showed that the FTIR spectrum of adsorbed CO on P25 is composed of two parts. The first part (2210-2165 cm^{-1}) is mainly due to CO adsorbed on Ti^{4+} sites present on the different faces and defects of anatase, which is the predominant phase (~85%) of P25. The intensity of the various components depends upon the dehydration state of the surface, as highlighted by the systematic study of samples activated at different temperatures. The second part (2149-2137 cm^{-1}) is associated with CO adsorbed on rutile (~15%). This assignment is proven by the predominance of these bands in the spectrum of CO adsorbed on the pure rutile component of P25, obtained by complete dissolution of the anatase phase with an HF solution, and by their absence in the pure anatase sample.

The 2149 cm^{-1} band has been tentatively assigned to CO adsorbed via carbon end on Ti^{4+} sites present on an extended face of rutile characterized by very low polarizing power, while the band at 2137 cm^{-1} is probably due to CO adsorbed via oxygen end.

The study of the effect of coverage on the IR spectrum of CO isotopic mixtures allowed to investigate the adsorbate-adsorbate (dipole-dipole) interactions between the parallel CO oscillators present on the different faces and to conclude that the faces of the anatase particles of P25 are very regular and extended. On the contrary, the dipole-dipole interaction is suppressed when adsorbed water is present on the surface.

These results concerning the spectroscopic properties of extended adlayers of parallel CO oscillators confirm the high crystalline character of P25, which seems to be the most relevant property differentiating this material from those synthesized in a different way.

The FTIR spectrum of adsorbed CO on nanoanatase, which is characterized by particles of smaller size, irregular contours and by the presence of a larger fraction of sites located on defects, is in full

agreement with the previous assignments. In fact the peaks ascribed to CO adsorbed on the different faces are broader, heavily overlapped and less intense, as expected for particles characterized by facelets of reduced extension whose regularity is interrupted by defects. The comparison of the spectra of P25 and nanoanatase, before and after interaction with CO, confirms also the higher Bronsted acidity of the bridged OH groups with respect to the terminal ones.

Finally, on the basis of the surface picture provided by CO adsorption on P25 (which is a mixture of anatase and rutile), on the pure rutile fraction of P25 and on nanoanatase, we can conclude that the main spectral features of CO on P25 can be found separately in the pure anatase and rutile phases (although with different bandwidths). This suggests that no apparent interaction between the anatase and the rutile components of P25 with formation of new peculiar structures characteristic of anatase-rutile junctions is observable. Moreover, we showed the FTIR spectra of CO adsorbed on P25 are not dominated by the bands assigned to rutile, as it would be expected if the P25 particles were covered by a rutile layer. These results contribute to the long debate present in the literature on this topic, excluding the presence of a rutile layer on the surface of the anatase particles[13] and supporting the HRTEM measurements which have apparently demonstrated that P25 does not show the coexistence of more than one crystalline phase on each individual particle.[10]

Acknowledgements. Dr. G. Agostini is acknowledged for the acquisition of the HRTEM images. The work has been supported by the Italian MIUR through the FIRB Project RBAP115AYN “Oxides at the nanoscale: multifunctionality and applications” and by Ateneo-Compagnia di San Paolo-2011- 1A line, ORTO11RRT5 project.

Supporting Information Available. Details of the thermogravimetric analysis on the P25 sample and computational parameters. This material is available free of charge via the Internet at http://pubs.acs.org.

Author Information. Corresponding author e-mail address: lorenzo.mino@unito.it

Table 1. Phase composition in weight percentage of anatase (anat) and rutile (rut), particle dimension (d) calculated from XRD and BET surface area of the investigated samples.

Sample	$\%wt_{anat}$	$\%wt_{rut}$	d_{anat} (nm)	d_{rut} (nm)	BET surface area (m^2/g)
P25	83	17	26	42	61
P25HF	3	97	-	47	22
Nanoanatase	97	3	16	-	140

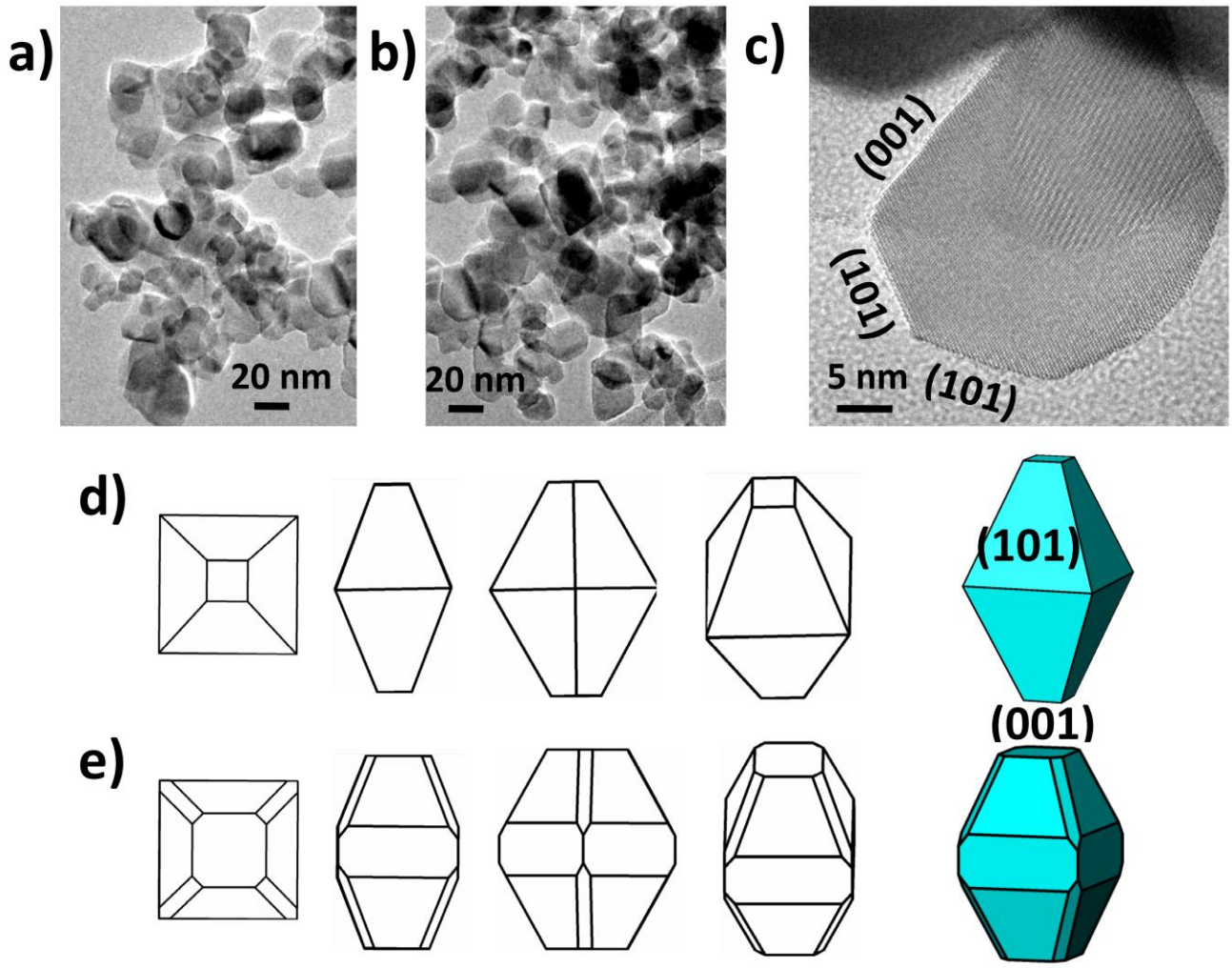

Figure 1. **a-b)** Low magnification HRTEM images of Degussa P25 particles. **c)** High magnification HRTEM image of a nearly isolated anatase particle of P25 in which the interference fringes originated by the (101) and (001) planes are clearly visible. **d)** Different rotated views of the truncated bipyramid obtained from the Wulff construction for anatase.[30] **e)** Different rotated views of a more complex polyhedron, containing also the (100) and (112) surfaces, which can better represent the actual morphology of the P25 particles reported in the HRTEM images. The adoption of a more complex morphology with respect to the Wulff equilibrium construction is justified by considering the non equilibrium conditions of the P25 synthesis.

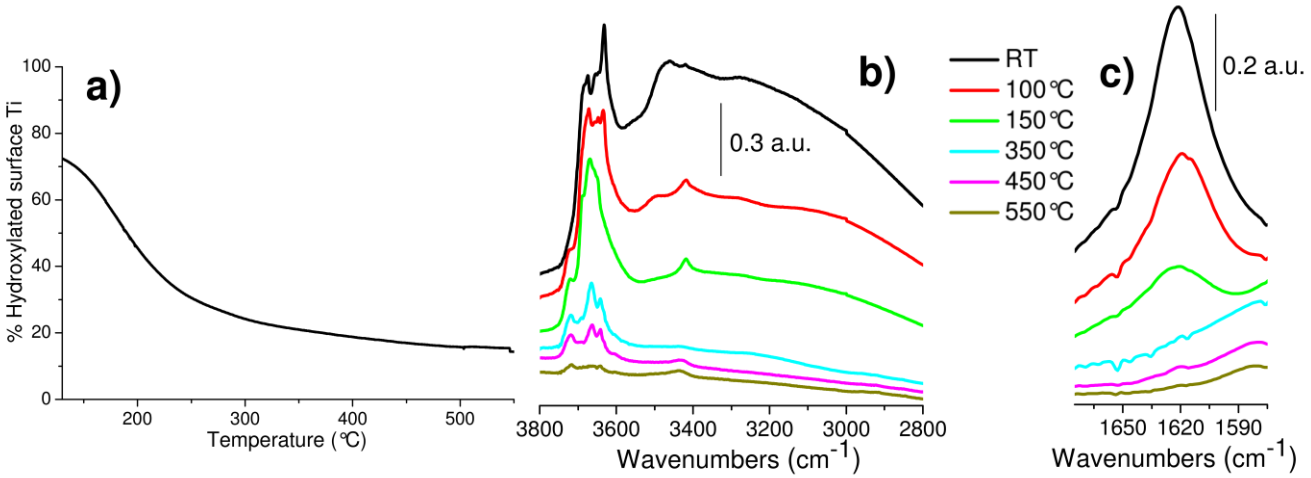

Figure 2. a) Percentage of hydroxylated surface Ti atoms as a function of the heating temperature calculated from TGA data. **b)** FTIR spectra showing the OH stretching region of P25 samples outgassed for 30 minutes at increasing temperatures**. c)** As part b) for the H_2O bending region.

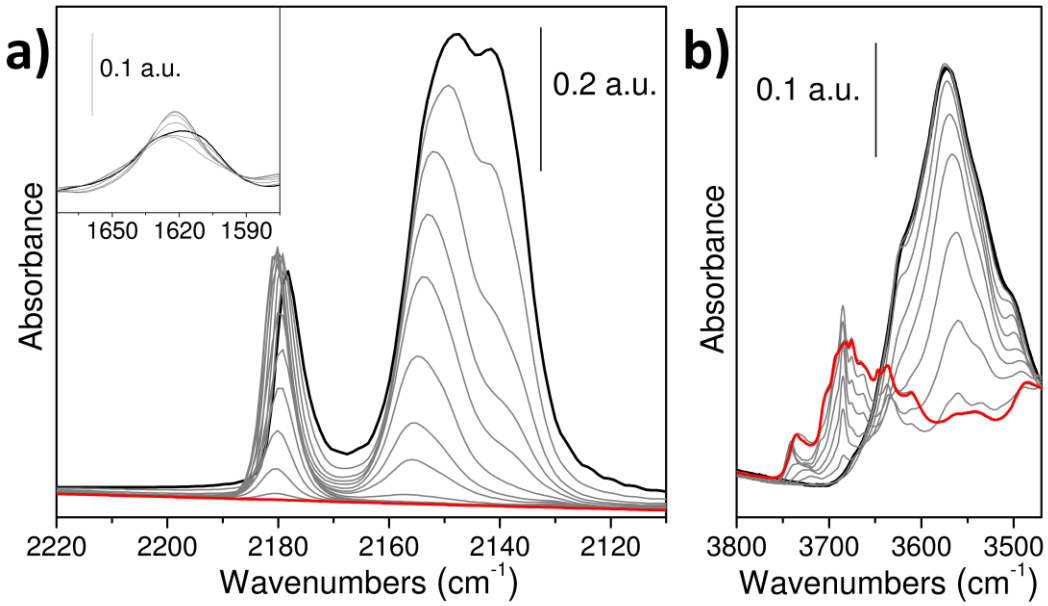

Figure 3. a) FTIR spectra, recorded at 60 K, of CO adsorbed at progressively decreasing coverages on P25 surface poisoned with about 0.5 monolayer of adsorbed water. In the inset the H_2O bending region is reported. **b)** As part a) for the OH stretching region. The black curve refers to maximum coverage (40 mbar of CO), the red curve to complete CO outgassing.

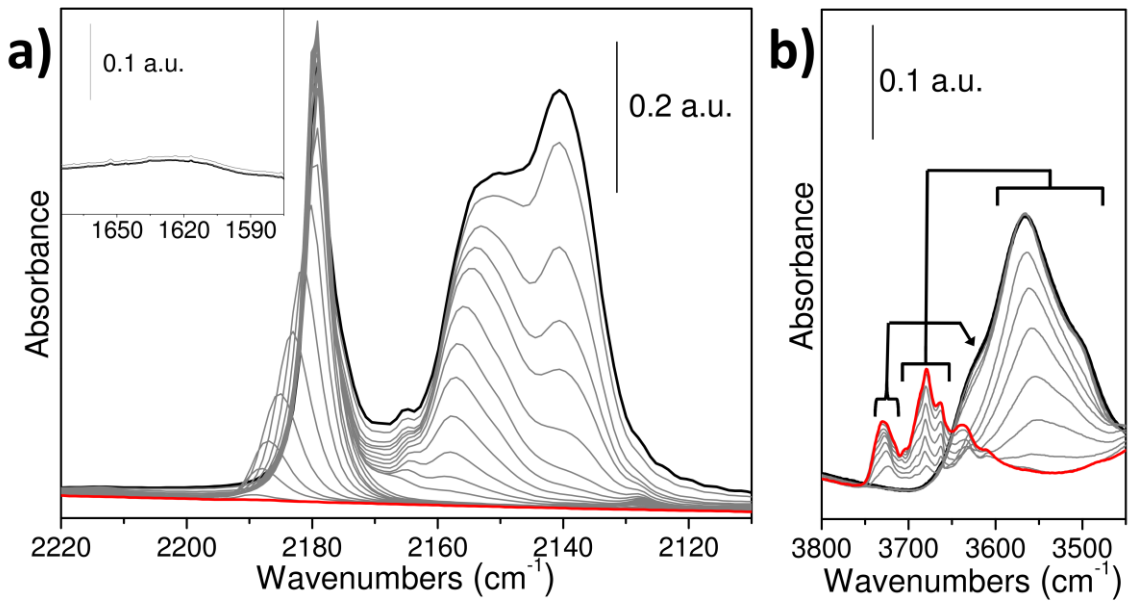

Figure 4. a) FTIR spectra, recorded at 60 K, of CO adsorbed at decreasing coverages on P25 nanocrystals previously outgassed for 1 hour at 400°C. In the inset the H_2O bending region is reported. **b)** As part a) for the OH stretching region. For a more detailed discussion of the OH shift assignment see the Supporting Information. The black curve refers to maximum coverage (40 mbar of CO), the red curve to complete CO outgassing.

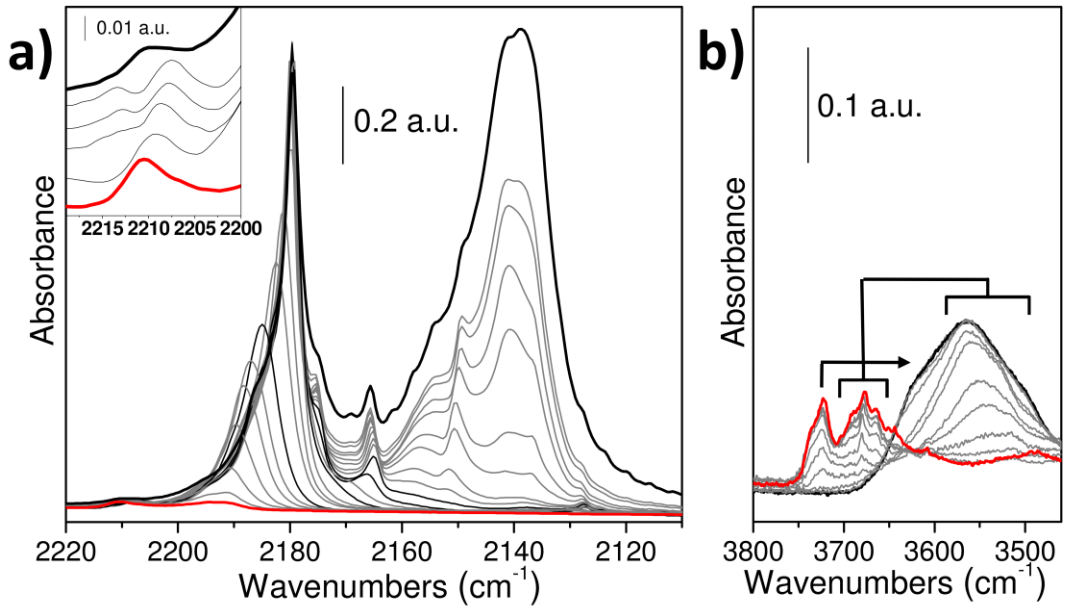

Figure 5. a) FTIR spectra, recorded at 60 K, of CO adsorbed at decreasing coverages on P25 nanocrystals previously outgassed for 5 hour at 500°C. In the inset a magnification of the weak signals in the 2220-2200 cm^{-1} range is reported. **b)** As part a) for the OH stretching region. The black curve refers to maximum coverage (40 mbar of CO), the red curve to complete CO outgassing.

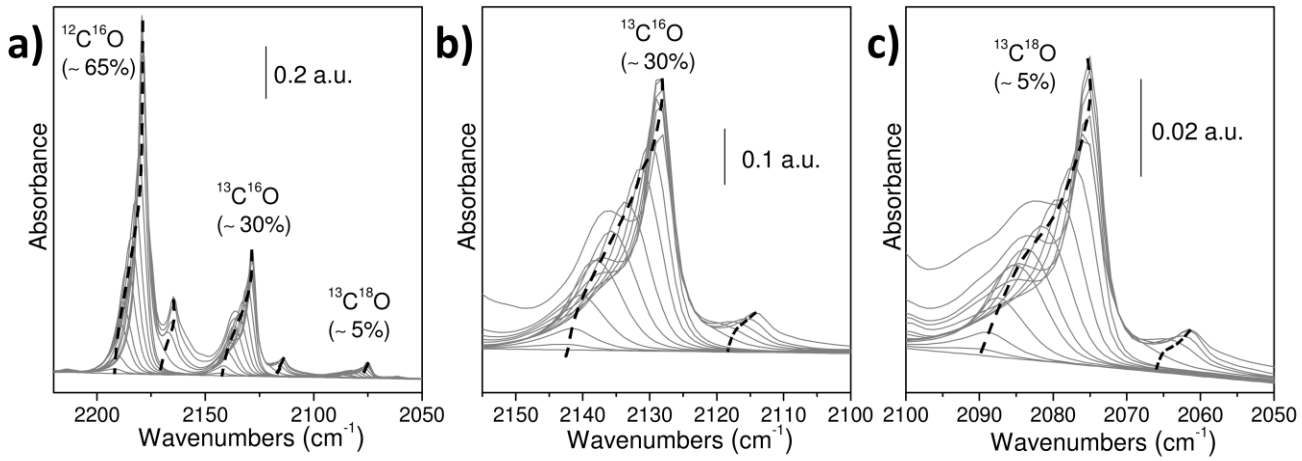

Figure 6. a) FTIR spectra, recorded at 60 K, of a $^{12}C^{16}O$-$^{13}C^{16}O$-$^{13}C^{18}O$ isotopic mixture adsorbed at progressively decreasing coverages on P25 nanocrystals previously outgassed at 500°C. **b)** Magnification of the $^{13}C^{16}O$ stretching region. **c)** Magnification of the $^{13}C^{18}O$ stretching region. The spectra at high CO coverages, when also physisorbed CO is present, are not shown for the sake of clarity The dashed black lines intend to help the reader to follow the position of the band maxima for the different coverages.

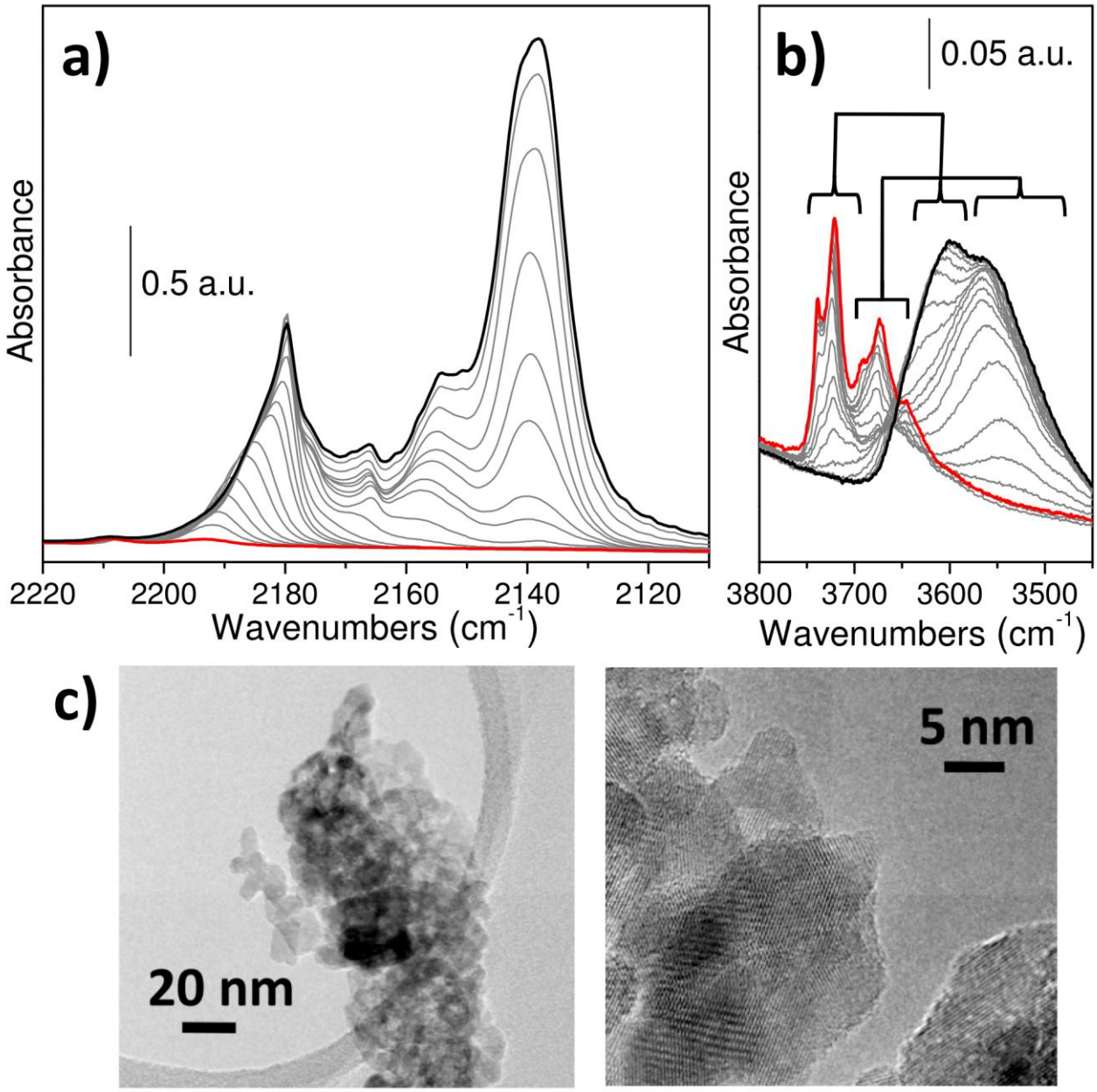

Figure 7. a) FTIR spectra, recorded at 60 K, of CO adsorbed at progressively decreasing coverages on nanoanatase previously outgassed at 500°C. **b)** As part a) for the OH stretching region. The black curve refers to maximum coverage (40 mbar of CO), the red curve to complete CO outgassing. **c)** HRTEM images of nanoanatase particles.

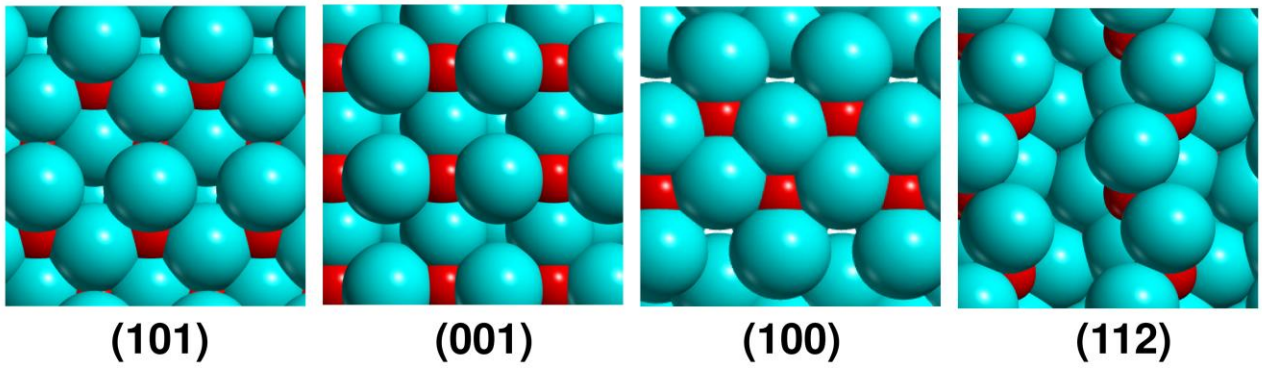

Figure 8. Top view of the most frequently exposed anatase faces, which represent the great majority of the P25 surface. Cyan spheres represent oxygen atoms, while red spheres represent titanium atoms. The surfaces were optimized using the PBE0 functional (see the Supporting Information for the computational details).

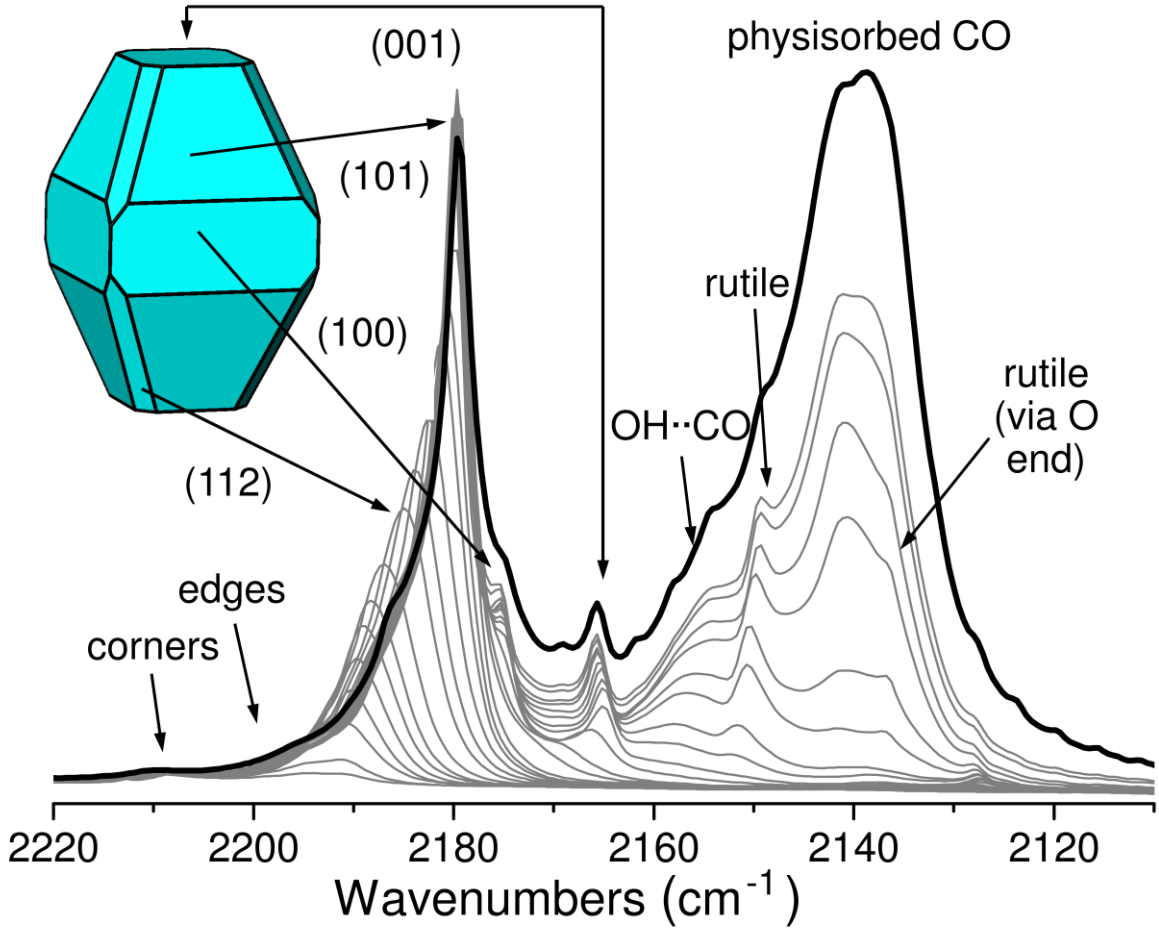

Figure 9. Assignment of the FTIR spectra of CO adsorbed at 60 K on P25. Please note that the assignment of the (100) and (112) surfaces in only tentative.

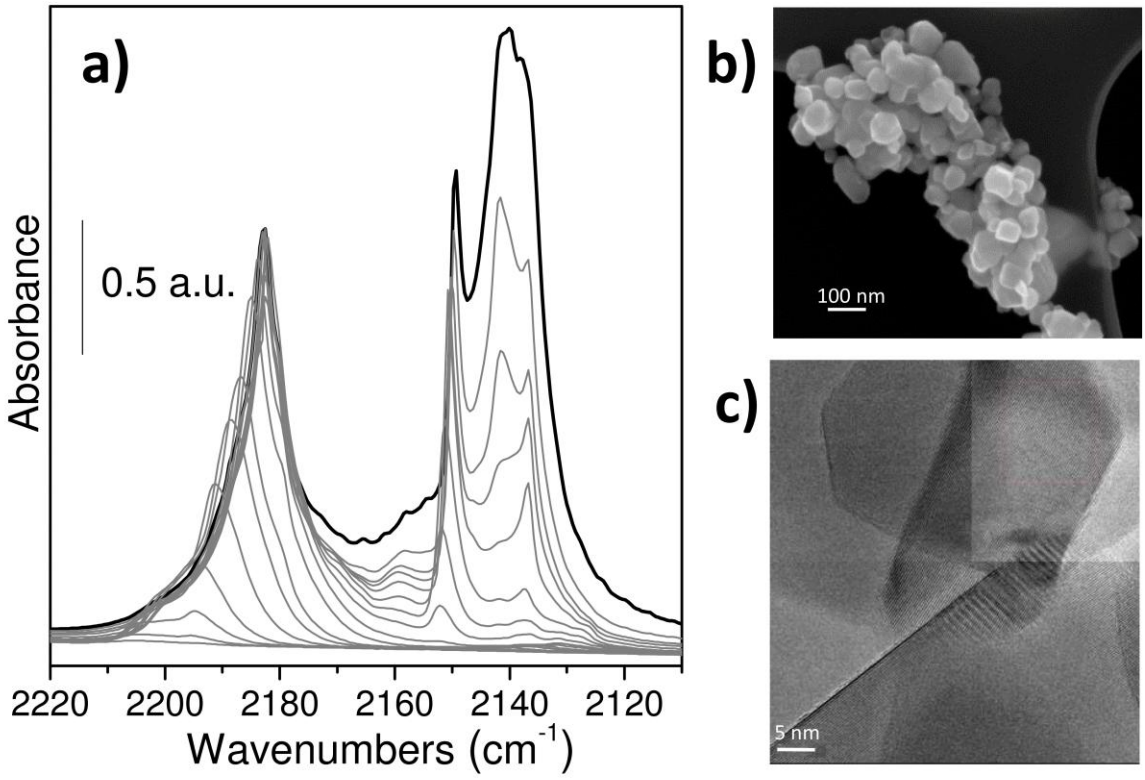

Figure 10. a) FTIR spectra, recorded at 60 K, of CO adsorbed at progressively decreasing coverages on P25 rutile particles previously outgassed at 500°C. **b)** FESEM image of the P25 rutile particles. **c)** HRTEM image of the P25 rutile particles. The rutile particles were obtained by etching P25 with an HF solution.

Table of Contents (TOC) Graphic.

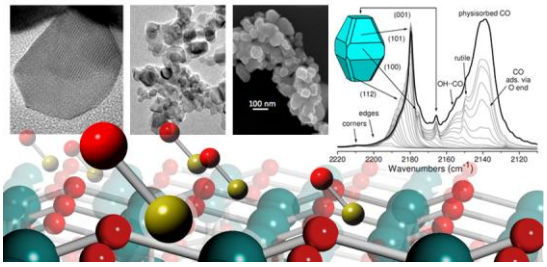

References

(1) Fujishima, A.; Zhang, X. T.; Tryk, D. A. *Surf. Sci. Rep.* **2008**, *63*, 515-582.

(2) Gratzel, M. *J. Photochem. Photobiol. C: Photochem Rev,* **2003**, *4*, 145-153.

(3) Diebold, U.; Lehman, J.; Mahmoud, T.; Kuhn, M.; Leonardelli, G.; Hebenstreit, W.; Schmid, M.; Varga, P. *Surf. Sci.* **1998**, *411*, 137-153.

(4) Enevoldsen, G. H.; Pinto, H. P.; Foster, A. S.; Jensen, M. C. R.; Hofer, W. A.; Hammer, B.; Lauritsen, J. V.; Besenbacher, F. *Phys. Rev. Lett.* **2009**, *102*, 4.

(5) Lindsay, R.; Wander, A.; Ernst, A.; Montanari, B.; Thornton, G.; Harrison, N. M. *Phys. Rev. Lett.* **2005**, *94*, 4.

(6) Cabailh, G.; Torrelles, X.; Lindsay, R.; Bikondoa, O.; Joumard, I.; Zegenhagen, J.; Thornton, G. *Phys. Rev. B* **2007**, *75*, 4.

(7) Harrison, N. M.; Wang, X. G.; Muscat, J.; Scheffler, M. *Faraday Discuss.* **1999**, *114*, 305-312.

(8) Diebold, U. *Surf. Sci. Rep.* **2003**, *48*, 53-229.

(9) Spoto, G.; Morterra, C.; Marchese, L.; Orio, L.; Zecchina, A. *Vacuum* **1990**, *41*, 37-39.

(10) Datye, A. K.; Riegel, G.; Bolton, J. R.; Huang, M.; Prairie, M. R. *J. Solid State Chem.* **1995**, *115*, 236-239.

(11) Martra, G. *Appl. Catal. A-Gen.* **2000**, *200*, 275-285.

(12) Ohno, T.; Sarukawa, K.; Tokieda, K.; Matsumura, M. *J. Catal.* **2001**, *203*, 82-86.

(13) Bickley, R. I.; Gonzalezcarreno, T.; Lees, J. S.; Palmisano, L.; Tilley, R. J. D. *J. Solid State Chem.* **1991**, *92*, 178-190.

(14) Martin, S. T.; Herrmann, H.; Choi, W. Y.; Hoffmann, M. R. *J. Chem. Soc.-Faraday Trans.* **1994**, *90*, 3315-3322.

(15) Kolen'ko, Y. V.; Churagulov, B. R.; Kunst, M.; Mazerolles, L.; Colbeau-Justin, C. *Appl. Catal. B-Environ.* **2004**, *54*, 51-58.

(16) Emilio, C. A.; Litter, M. I.; Kunst, M.; Bouchard, M.; Colbeau-Justin, C. *Langmuir* **2006**, *22*, 3606-3613.

(17) Hurum, D. C.; Agrios, A. G.; Gray, K. A.; Rajh, T.; Thurnauer, M. C. *J. Phys. Chem. B* **2003**, *107*, 4545-4549.

(18) Hurum, D. C.; Gray, K. A.; Rajh, T.; Thurnauer, M. C. *J. Phys. Chem. B* **2005**, *109*, 977-980.

(19) Hadjiivanov, K. I.; Klissurski, D. G. *Chem. Soc. Rev.* **1996**, *25*, 61-69.

(20) Scarano, D.; Spoto, G.; Bordiga, S.; Zecchina, A.; Lamberti, C. *Surf. Sci.* **1992**, *276*, 281-298.

(21) Pacchioni, G.; Ferrari, A. M.; Bagus, P. S. *Surf. Sci.* **1996**, *350*, 159-175.

(22) Sorescu, D. C.; Yates, J. T. *J. Phys. Chem. B* **1998**, *102*, 4556-4565.

(23) Scaranto, J.; Giorgianni, S. *Mol. Phys.* **2008**, *106*, 2425-2430.

(24) Scaranto, J.; Giorgianni, S. *Theochem-J. Mol. Struct.* **2008**, *858*, 72-76.

(25) Scaranto, J.; Giorgianni, S. *Mol. Phys.* **2009**, *107*, 1997-2003.

(26) Mino, L.; Ferrari, A. M.; Lacivita, V.; Spoto, G.; Bordiga, S.; Zecchina, A. *J. Phys. Chem. C* **2011**, *115*, 7694-7700.

(27) Spoto, G.; Gribov, E. N.; Ricchiardi, G.; Damin, A.; Scarano, D.; Bordiga, S.; Lamberti, C.; Zecchina, A. *Prog. Surf. Sci.* **2004**, *76*, 71-146.

(28) Spurr, R. A.; Myers, H. *Anal. Chem.* **1957**, *29*, 760-762.

(29) Deiana, C.; Fois, E.; Coluccia, S.; Martra, G. *J. Phys. Chem. C* **2010**, *114*, 21531-21538.

(30) Selloni, A. *Nat. Mater.* **2008**, *7*, 613-615.

(31) Morterra, C. *J. Chem. Soc.-Faraday Trans.* **1988**, *84*, 1617-1637.

(32) Soria, J.; Sanz, J.; Sobrados, I.; Coronado, J. M.; Maira, A. J.; Hernandez-Alonso, M. D.; Fresno, F. *J. Phys. Chem. C* **2007**, *111*, 10590-10596.

(33) Arrouvel, C.; Digne, M.; Breysse, M.; Toulhoat, H.; Raybaud, P. *J. Catal.* **2004**, *222*, 152-166.

(34) Finnie, K. S.; Cassidy, D. J.; Bartlett, J. R.; Woolfrey, J. L. *Langmuir* **2001**, *17*, 816-820.

(35) Posternak, M.; Baldereschi, A.; Delley, B. *J. Phys. Chem. C* **2009**, *113*, 15862-15867.

(36) Zecchina, A.; Scarano, D.; Bordiga, S.; Ricchiardi, G.; Spoto, G.; Geobaldo, F. *Catal. Today* **1996**, *27*, 403-435.

(37) Hadjiivanov, K.; Lamotte, J.; Lavalley, J. C. *Langmuir* **1997**, *13*, 3374-3381.

(38) Panayotov, D. A.; Burrows, S. P.; Yates, J. T.; Morris, J. R. *J. Phys. Chem. C* **2011**, *115*, 22400-22408.

(39) Stevanovic, A.; Buttner, M.; Zhang, Z.; Yates, J. T. *J. Am. Chem. Soc.* **2012**, *134*, 324-332.

(40) Minella, M.; Faga, M. G.; Maurino, V.; Minero, C.; Pelizzetti, E.; Coluccia, S.; Martra, G. *Langmuir* **2010**, *26*, 2521-2527.

(41) Arean, C. O.; Palomino, G. T.; Zecchina, A.; Spoto, G.; Bordiga, S.; Roy, P. *PCCP Phys. Chem. Chem. Phys.* **1999**, *1*, 4139-4140.

(42) Hadjiivanov, K.; Reddy, B. M.; Knozinger, H. *Appl. Catal. A-Gen.* **1999**, *188*, 355-360.

(43) Zecchina, A.; Scarano, D.; Garrone, E. *Surf. Sci.* **1985**, *160*, 492-508.

(44) Hadjiivanov, K.; Penkova, A.; Centeno, M. A. *Catal. Commun.* **2007**, *8*, 1715-1718.

(45) Zecchina, A.; Scarano, D.; Bordiga, S.; Spoto, G.; Lamberti, C. In *Advances in Catalysis, Vol 46*; Academic Press Inc: San Diego, 2001; Vol. 46, p 265-397.

(46) Sun, C.; Liu, L.-M.; Selloni, A.; Lu, G. Q.; Smith, S. C. *J. Mater. Chem.* **2010**, *20*, 10319-10334.

(47) Xu, M. C.; Gao, Y. K.; Moreno, E. M.; Kunst, M.; Muhler, M.; Wang, Y. M.; Idriss, H.; Woll, C. *Phys. Rev. Lett.* **2011**, *106*, 4.

(48) Hadjiivanov, K. *Appl. Surf. Sci.* **1998**, *135*, 331-338.

(49) Ferretto, L.; Glisenti, A. *Chem. Mat.* **2003**, *15*, 1181-1188.

(50) Panayotov, D. A.; Burrows, S.; Mihaylov, M.; Hadjiivanov, K.; Tissue, B. M.; Morris, J. R. *Langmuir* **2010**, *26*, 8106-8112.